An isotopic substitution study of $NiCl_2 - KCl$ and $ZnCl_2 - KCl$ binary molten salt mixtures

1996 J. Phys.: Condens. Matter 8 3733

(http://iopscience.iop.org/0953-8984/8/21/003)

J. Phys.: Condens. Matter **8** (1996) 3733–3754. Printed in the UK

An isotopic substitution study of $NiCl_2$–KCl and $ZnCl_2$–KCl binary molten salt mixtures

Y S Badyal† and R A Howe

Physics and Astronomy Department, University of Leicester, Leicester LE1 7RH, UK

Received 10 August 1995, in final form 8 February 1996

Abstract. The scattering from $^{x}NiCl_2$–KCl binary molten salt mixtures of nominally two thirds alkali halide concentration, where $x =$ 'natural', 'zero-scattering' and '62' enrichments of nickel, has been measured by time-of-flight neutron diffraction on ISIS LAD. A complementary experiment was performed on molten $ZnCl_2$–KCl samples, also of nominally two thirds alkali halide concentration, using isotopic substitution of chlorine. In the case of $NiCl_2$–KCl, the results indicate a large first sharp diffraction peak (FSDP) in $S_{Ni-Ni}(Q)$ and $S_{Ni-Cl}(Q)$ but not in $S_{K-K}(Q)$. Reverse Monte Carlo (RMC) modelling indicates a well-ordered, almost regularly tetrahedral local structure for the Ni^{2+} ion, the preponderance of large K^+ ions as next-nearest neighbours to the metal cation and the apparent association of this with enhanced intermediate-range order (IRO) in the mixtures. The results confirm the findings of the initial composition study of this system and provide further support for the suggestion that enhanced IRO arises from ordering between tetrahedral units and alkali counter-ions. Modelling of the $ZnCl_2$–KCl data suggests a strong similarity with molten $NiCl_2$–KCl even though the pure $NiCl_2$ and $ZnCl_2$ molten salt structures are confirmed to be dissimilar.

1. Introduction

In a previous paper [1], the results of a composition study of binary molten salt mixtures of divalent metal chlorides with alkali chlorides were described. The main conclusion was that the degree of structural modification was dependent on the relative size and polarizing power of the alkali cation. The mixtures of $NiCl_2$, and $ZnCl_2$, with LiCl simply appeared to be admixtures of the two pure salt structures. In contrast, adding KCl to $NiCl_2$ led to the following structural changes.

(i) A more ordered local structure around the Ni^{2+} ion with the alkali cation appearing to occupy disordered sites.

(ii) A transition to a more regularly tetrahedral local coordination for the metal cation from one which is best described as disordered octahedral (with 1–2 vacancies) in pure molten $NiCl_2$.

(iii) The dominance of the short-range anion structure by the metal cation, which is consistent with the formation of discrete $NiCl_4^{2-}$ tetrahedral units.

(iv) An enhanced FSDP at $Q \sim 1$ Å^{-1} in the total structure factor, particularly at higher KCl concentrations, implying increased IRO.

Similar findings were reported by Allen *et al* [2] in their composition study of $ZnCl_2$–KCl melts with one important difference: little change was observed in the local geometry

† Present address: Interfacultair Reactor Instituut, Mekelweg 15, 2629 JB Delft, The Netherlands (e-mail: Badyal@iri.tudelft.nl).

0953-8984/96/213733+22$19.50

of the Zn^{2+} ion, which remains almost regularly tetrahedral just as in pure molten $ZnCl_2$ [3]. Intriguingly, Allen and co-workers also reported that enhancement of the FSDP seems to reach its maximum near the 2/3 alkali halide concentration. At this critical composition, it is possible for the melt to consist exclusively of tetrahedral $ZnCl_4^{2-}$ units and K^+ ions. Pure molten $ZnCl_2$ has a prominent FSDP in the Zn–Zn partial structure factor (PSF) [3] and it has been suggested by Wood and Howe [4] that this correlation is due to the angular dependence of interionic forces giving rise to IRO involving corner-linked $ZnCl_4^{2-}$ tetrahedral units. Given this explanation, and contrary to the observations of Allen *et al*, the breakdown of the $ZnCl_2$ network structure upon the addition of alkali halide might have been expected to lead to a marked reduction in the size of the FSDP. In [1], a simple model was proposed for molten $NiCl_2$–KCl mixtures in which the large K^+ ions act to both space apart and charge order $NiCl_4^{2-}$ units, thus giving rise to a less random, more 'lattice-like' structure and hence increased IRO involving the metal cations. Such a model, it seems, could apply equally well to molten $ZnCl_2$–KCl.

The central aim of the research described in this paper was to study, in detail, the nature of the enhanced IRO in the mixtures. The simple model involving charge ordering between tetrahedral units and alkali counter-ions suggests there should be a sizeable FSDP arising not only from the metal–metal correlation but possibly also from metal–alkali and alkali–alkali correlations. By isotopic substitution of nickel in (nominally) $NiCl_2 + 2KCl$ melts it was possible to ascertain the precise contributions of some of the partials to the enhanced FSDP in the total scattering. In addition, a chlorine substitution study of (nominally) $ZnCl_2 + 2KCl$ melts was undertaken in an attempt to obtain details of the anion structure and, it was hoped (bearing in mind the similarities between the two systems), information complementary to that available from the nickel isotopes experiment. RMC modelling made it possible to extract the maximum structural information from the data. The wider aim of this study was to confirm the general trends highlighted in the earlier composition studies of these systems.

2. Theory

The aim of a neutron diffraction experiment is to determine the total structure factor, $F(Q)$. This is defined for a two-component system with atoms of type a and b by the following relation:

$$F(Q) = c_a^2 b_a^2 (S_{aa}(Q) - 1) + c_b^2 b_b^2 (S_{bb}(Q) - 1) + 2c_a c_b b_a b_b (S_{ab}(Q) - 1) \tag{1}$$

where c_α is the concentration and b_α is the coherent scattering length of species α. The $S_{\alpha\beta}(Q)$ terms are the PSFs according to the definition of Faber and Ziman [5]. Because b can vary significantly even between isotopes of the same element, it is possible to obtain details of the partial structures using the well-established technique of isotopic substitution. This involves measuring the scattering from samples with the same chemical composition but different isotopic enrichments (with known coherent scattering lengths) and solving the resulting set of linear simultaneous equations.

$S_{\alpha\beta}(Q)$ is related to the pair distribution function, $g_{\alpha\beta}(r)$, by Fourier transformation as shown below:

$$g_{\alpha\beta}(r) = 1 + \frac{1}{2\pi^2 \rho_0} \int_0^\infty Q^2 (S_{\alpha\beta}(Q) - 1) \frac{\sin(Qr)}{Qr} \, \mathrm{d}Q \tag{2}$$

where ρ_0 is the number density. From this an expression for the Fourier transform (FT) of $F(Q)$, known as the total pair distribution function or $G(r)$, can be obtained thus:

$$G(r) = 1 + c_a^2 b_a^2 (g_{aa}(r) - 1) + c_b^2 b_b^2 (g_{bb}(r) - 1) + 2c_a c_b b_a b_b (g_{ab}(r) - 1). \tag{3}$$

Not surprisingly, $G(r)$ is a linear sum of the various partial structures, weighted for concentration and scattering, just as in the original $F(Q)$ function.

Although the precise form of the equations shown is only valid for pure molten salts containing two types of atom, such as $NiCl_2$, they can be generalized for any number of components.

3. Experimental details

The mixtures were prepared from the isotopically enriched single salts heated gently under vacuum to minimize moisture content. After weighing out the appropriate amounts of the dried pure salts, the samples were 'pre-mixed' by heating to at least 25 °C above the liquidus, as indicated in the phase diagrams for $NiCl_2$–KCl [6] and $ZnCl_2$–KCl [7], and maintained at that temperature for at least 18 hours. The prepared samples were loaded into fused quartz containers of approximately 6 mm internal diameter and 1 mm wall thickness before being sealed off under an argon pressure of ∼0.5 atm at room temperature. Full details of the sample preparation procedure are given by Allen *et al* [2].

The scattering from three isotopically enriched samples of molten $NiCl_2$–KCl ('natural', 'zero-scattering' and '62' nickel enrichments), at a single nominal composition of 67% alkali halide and a temperature of 650 °C, was measured by time-of-flight neutron diffraction on ISIS LAD. In a separate LAD experiment, measurements were made on three samples of molten $ZnCl_2$–KCl, also of nominally 67% alkali halide concentration, enriched in ^{35}Cl, ^{37}Cl and ^{mix}Cl (an ∼50:50 mixture of the two chlorine isotopes), all at a temperature of 480 °C. As usual, multiple scans were taken for each sample to monitor any structural changes in sample or container due to incomplete mixing or chemical attack during data collection. Only scans that agreed to within statistical error were added together. Phase separation in the ^{37}Cl-enriched sample was evident in the form of persistent, small Bragg peaks that gradually decreased in size as the temperature was raised from 480 °C and then increased again upon cooling. This sample was carefully recovered from its container and crushed to re-mix it before it was re-tubed for a successful second measurement. Unfortunately, this problem meant that there was no time remaining on the LAD instrument to make measurements for a 'natural' $ZnCl_2$–KCl sample. In each experiment, data were collected for the empty container, furnace and instrument backgrounds as well as a vanadium calibration.

The raw data were analysed using the ATLAS package [8], with furnace corrections being applied. The SUBSELF [9] routine was used to remove slopes at high Q and improve the agreement between detector groups. Composite $F(Q)$s were obtained by merging those Q-ranges of adjacent detector groups which matched well. Other than for the ±5° bank, there was good agreement between opposite pairs of detector groups. The lack of isothermal compressibility data precluded the use of the long-wavelength limit as a check on normalization. The missing low-Q portion of the data was simply extrapolated but, because of the Q^2-dependence of the Fourier transform, this makes little difference to the real-space picture. The $G(r)$ functions were obtained by Fourier transformation of $F(Q)$ data smoothed at high Q. No window function was used. Comparison of the $G(r)$ from smoothed and unsmoothed $F(Q)$ data confirmed that mainly Fourier ripple was removed with marginal effect on real peaks. No obvious signs of excess or deficit of container scattering were noted in the $G(r)$ data.

The isotopic enrichments were checked, using the mass spectrometer at the Bristol isotope preparation unit, prior to data analysis, and are shown in table 1. Because of the lack of published measurements, the number density initially used for molten $NiCl_2$–KCl was linearly interpolated from those of the pure salt endpoints at 1040 °C. The consistent

Table 1. Coherent scattering lengths for the isotopic enrichments used in each sample. The individual scattering lengths of each isotope were taken from Sears [10].

	$NiCl_2$–KCl			$ZnCl_2$–KCl		
	^{nat}Ni	^{zero}Ni	^{62}Ni	^{35}Cl	^{mix}Cl	^{37}Cl
(fm)	10.31	1.045	−6.75	11.59	7.41	3.68

Table 2. Comparison of crystal ionic radii for the divalent metal cation in the solid phases, and first-peak positions in $G(r)$ [1] for the liquid phases, of $NiCl_2$ and $ZnCl_2$. The symbol M denotes the metal cation. The almost identical values suggest a close similarity in metal-ion sizes.

Salt	Ionic radii (Å)	r_{M-Cl} (Å)
$NiCl_2$	0.72	2.28 ± 0.02
$ZnCl_2$	0.74	2.29 ± 0.02

renormalization factor of approximately 0.95 found for all three $NiCl_2$–KCl samples allowed a crude correction to be made to this figure. Given the similarity expected from the almost identical metal-ion sizes in the two systems (see table 2), the corrected density value of 0.0285 $Å^{-3}$ is in satisfyingly good agreement with the known value of 0.028 $Å^{-3}$ for the $ZnCl_2$–KCl mixture.

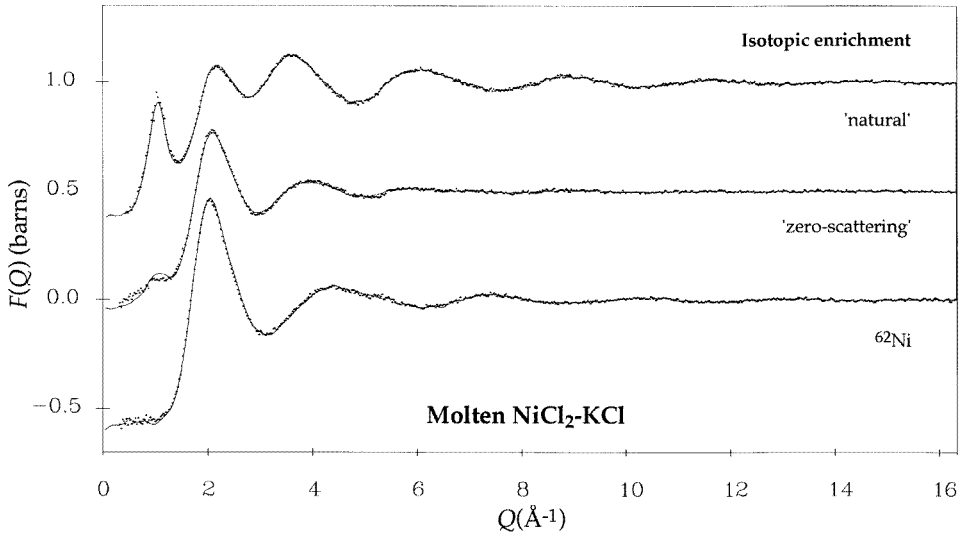

Figure 1. Total structure factor data (dotted curves) for the $NiCl_2$–KCl samples compared with their respective RMC fits (solid curves). The deviations between model and data are most pronounced at low Q, but this is to be expected since corrections for absorption and inelasticity are greatest in this region.

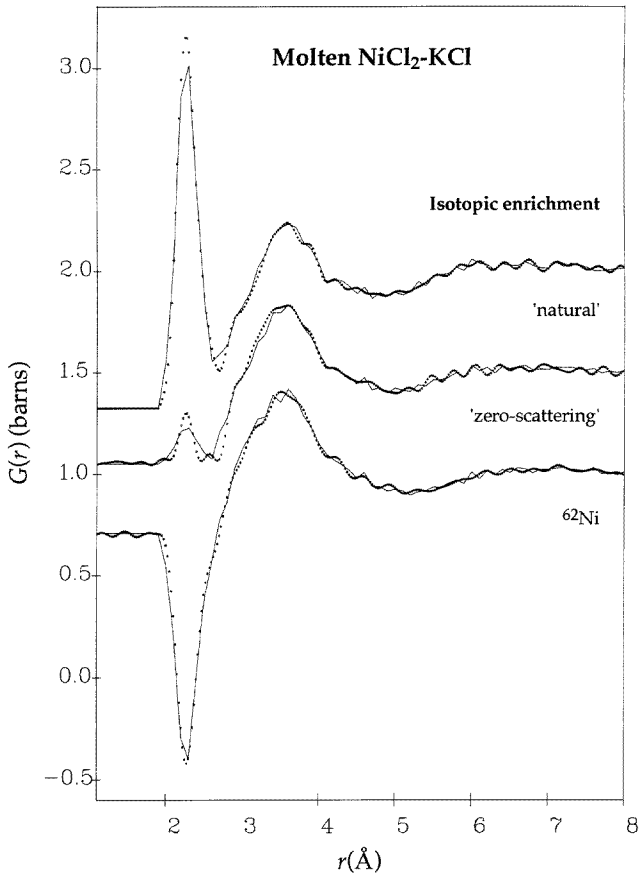

Figure 2. Total pair distribution functions (dotted curves) for the $NiCl_2$–KCl samples compared against the corresponding RMC fits (solid curves). Note that the 'zero-scattering' sample clearly does not have a coherent scattering length of exactly zero for nickel because a small Ni–Cl principal peak is still visible at $r \sim 2.3$ Å.

4. Discussion

4.1. The structure of molten $NiCl_2$–KCl

The total structure factors and corresponding total pair distribution functions for the three $NiCl_2$–KCl samples are shown in figures 1 and 2, respectively. In order to extract the maximum structural information, the RMC method was used to model the data. Since the RMC method and its application are extensively described elsewhere (see, e.g., [11]), a brief outline will suffice here. Basically, RMC modelling is a variant of the standard Metropolis Monte Carlo algorithm and differs only in that a fit directly to the diffraction data is minimized, rather than the total potential energy. The starting configuration was always a random one containing $N = 2400$ atoms satisfying the appropriate geometrical constraints. The dimensions of the simulation cube gave an effective simulation size of $r \sim 21.9$ Å (the maximum distance for calculating the model $G(r)$). Initially, modelling was confined to the real-space data in order to allow the closest-approach distances to be

fine tuned before restarting from a random configuration and fitting directly to the structure factors. As the model neared equilibrium, with χ^2 converging to a minimum, refinement of the fit by automatic renormalization of the data was allowed. The renormalization factor was usually close to unity (typically $\pm 2.5\%$). Statistically independent configurations, each separated by at least $2N$ accepted moves, were collected for averaging of their properties once the model had clearly reached equilibrium.

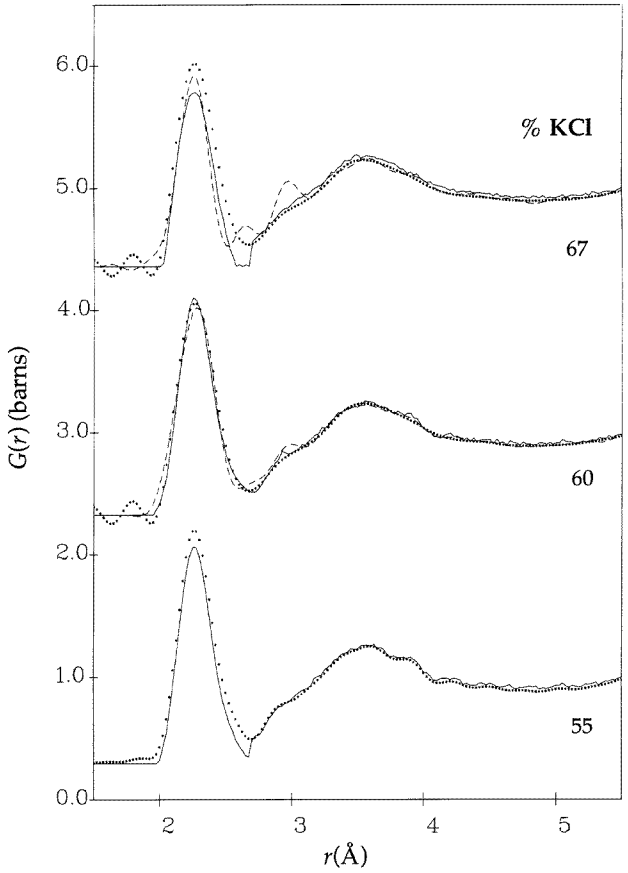

Figure 3. The effects of varying the composition on the RMC modelling of data (dotted) for the 'natural' molten $NiCl_2$–KCl sample. The real-space results for the fitting to $G(r)$ (solid curves) and directly to the total structure factor (dashed curves) are shown. The spurious peak at approximately 3 Å in the 67% KCl RMC fit to $F(Q)$ arises from the K–Cl partial.

Initial RMC modelling of the 'natural' sample alone (chosen to avoid possible misleading results from errors in isotopic enrichment) suggested that the nominal 2/3 alkali halide concentration was incorrect. Under-fitting of the first main peak in $G(r)$ resulted from modelling the real-space data, and a spurious spike in the leading edge of the RMC $g_{K-Cl}(r)$ partial was observed in subsequent modelling of the structure factor. These findings can be explained in terms of there being too few Ni^{2+} ions to allow a good match to the main Ni–Cl peak in real space and, conversely, too many K^+ ions, so these are pushed down to low r, where they have less effect on the back-transform, when fitting to the structure factor. Modifying the composition of the RMC model to 60% KCl led to a better fit to the first

peak in $G(r)$ and the disappearance of the spurious spike in $g_{K-Cl}(r)$. Reducing the alkali halide concentration yet further to 55% KCl produced a worse match to the main Ni–Cl peak in real space. RMC modelling thus clearly favours the 60% KCl concentration as being more correct (see figure 3). Confirmation of this finding was provided by subsequent chemical analysis of the entire 'natural' sample which estimated the composition, based on the Ni:K ratio, as $59 \pm 1\%$ KCl. Equilibrium configurations were collected for the RMC model obtained assuming a 60% KCl composition. Although this represents only a *provisional* model (henceforth known as model P) found by fitting to a single structure factor, it will prove useful later in highlighting the key features of the full model (henceforth known as model F) obtained by exploiting the complete set of isotopic data. Note that a provisional RMC model could also have been generated by fitting to the structure factor for the ^{62}Ni-enriched sample, but since we already had a model for the 'natural' sample this would only have incurred further and unnecessary computational expense.

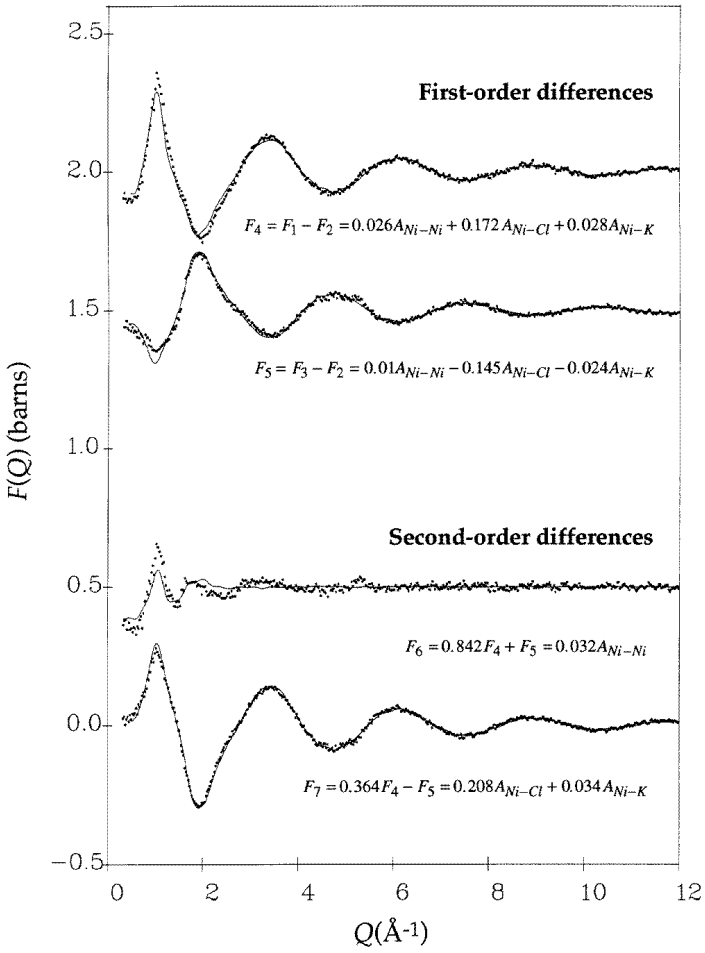

Figure 4. Comparison of the direct first- and second-order differences (dotted curves) against the model-F RMC solution (solid curves), for the $NiCl_2$–KCl data.

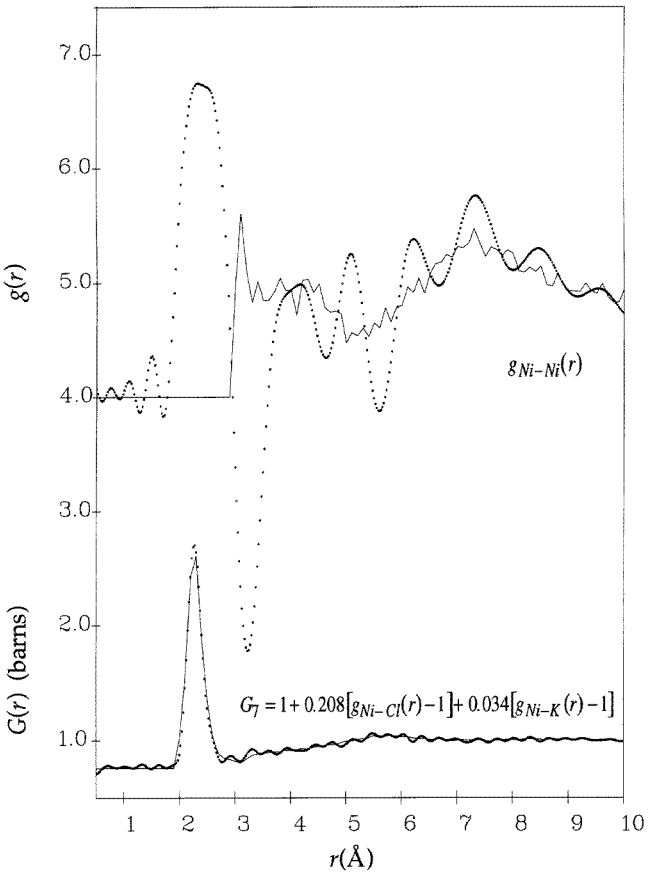

Figure 5. Comparison of the real-space functions obtained from the direct second-order differences (dotted curves) shown in figure 4 and the RMC solution (solid curves). Note that the Ni–Ni partial is clearly unphysical at low r and RMC modelling is essential to obtaining a realistic solution. The spurious peak and trough at $r \sim 2.3$ and 3.4 Å, respectively, appear to correspond to the features between $Q \sim 2$ and 6 Å^{-1} in F_6 (see figure 4) which are not modelled by RMC.

The results, after adopting the 60% KCl composition†, of a RMC fit simultaneously to all three $F(Q)$ data-sets are also shown in figures 1 and 2. Although the composition of the ^{62}Ni- and ^{zero}Ni-enriched samples has not been checked independently, the existence of a RMC model physically consistent with all three data-sets strongly suggests there is no significant deviation from the assumed 60% KCl concentration. The structure factors expressed in terms of the appropriate Faber–Ziman coefficients for 'natural' (F_1), 'zero-

† A deficit of 10% in the amount of KCl in these samples is quite plausible given the details of sample preparation. As usual [2], the vacuum-dried KCl was cast into solid pellets for easier handling, and the same batch of KCl used to prepare all the samples. However, solid KCl has a glassy appearance and can be difficult to distinguish from container quartz. It now appears that some fragments of quartz were inadvertently incorporated, in place of KCl, when making up the mixtures. Fortunately, the KCl-deficient samples resulting from this systematic error are not likely to differ greatly in composition from each other.

scattering' (F_2) and ^{62}Ni (F_3) enrichments are

$$F_1 = 0.03A_{Ni-Ni} + 0.192A_{Ni-Cl} + 0.032A_{Ni-K} + 0.312A_{Cl-Cl} + 0.103A_{Cl-K} + 0.008A_{K-K}$$

$$F_2 = 0.0003A_{Ni-Ni} + 0.02A_{Ni-Cl} + 0.003A_{Ni-K} + 0.312A_{Cl-Cl} + 0.103A_{Cl-K} + 0.008A_{K-K}$$

$$F_3 = 0.013A_{Ni-Ni} - 0.126A_{Ni-Cl} - 0.021A_{Ni-K} + 0.312A_{Cl-Cl} + 0.103A_{Cl-K} + 0.008A_{K-K}$$

where $A_{\alpha\beta}$ corresponds to $(S_{\alpha\beta}(Q) - 1)$. In figures 4 and 5, the RMC solution is compared to the direct first-order and second-order differences. Compared with straightforward isotopic differencing, the RMC method has the advantage of powerful additional constraints on ion size and density which ensure that the solution partials are physically consistent with each other. This is best illustrated (see figure 5) for the case of the Ni–Ni partial, which in principle can be obtained uniquely, where using RMC modelling enforces a physically realistic solution.

At this point, it must be stated that what follows next is a discussion of a particular (RMC) model generated using the limited amount of information contained in three structure factors. To derive uniquely the six partial structures that actually describe the system would of course require three additional structure factors that are not available to us. However, RMC modelling can compensate, to an indeterminate extent, for the missing information by using physical constraints. So examining our model, which has been obtained using the best available information, is likely to yield genuine insights into the structure of molten $NiCl_2$–KCl.

The RMC model-F partial structure factors are shown in figure 6 and, as expected, the unique $S_{Ni-Ni}(Q)$ partial exhibits a large peak at $Q \sim 1$ Å^{-1} which makes a substantial contribution to the FSDP in the total scattering and is much larger than in pure $NiCl_2$ [12]. Rather surprising is the presence of a trough, rather than a peak, at approximately the same position in the $S_{Ni-K}(Q)$ partial. The $S_{Ni-Cl}(Q)$ PSF also exhibits a greatly enhanced FSDP compared to that of the pure salt. However, this partial is not unique although the weighting of the Ni–Cl term in the second-order difference F_7 (figure 4) strongly suggests that it is almost correct. There appears to be no obvious low-Q peak in $S_{K-K}(Q)$, which is consistent with the lack of a FSDP in the total structure factor for the 'zero-scattering' sample (no significant contribution was expected from $S_{K-Cl}(Q)$ and $S_{Cl-Cl}(Q)$ because of the absence of low-Q peaks in the same partials for the pure salts).

Table 3. Next-nearest-neighbour coordinations of Ni^{2+} averaged over several equilibrium configurations (r_{max} of 6 Å in all cases) for molten $NiCl_2$–KCl. The error bars have been estimated from the variation in coordination number between successive RMC configurations, so the true errors in the mean values shown below are probably less than indicated.

	Mean coordination number	
Neighbour type	Model P	Model F
Ni^{2+}	3.5 ± 0.2	3.0 ± 0.2
K^+	6.3 ± 0.2	6.7 ± 0.2

In order to identify the structural features induced by the additional isotopic information, particularly regarding the Ni–Ni correlation, available to the full RMC model, it is helpful

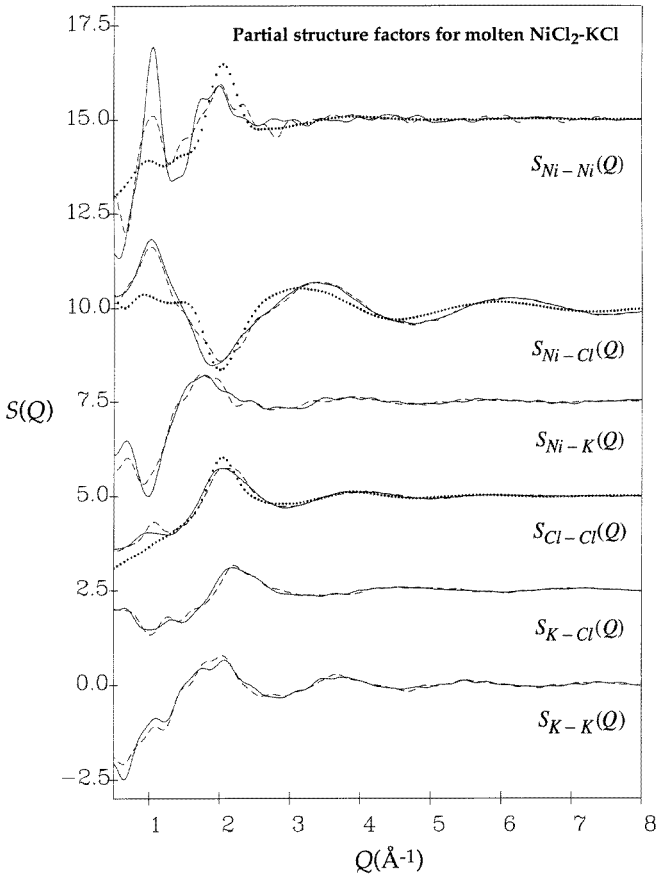

Figure 6. Comparison of RMC partial structure factors for model F (solid curves) and model P (dashed curves). The three PSFs for pure molten $NiCl_2$, from the isotopic study of Newport *et al* [12], are also shown as dotted curves.

to make comparisons with the provisional model. An advantage of this approach is that the differences between the two models will be virtually independent of the residual error in the estimated density (since the same value is used in both models). Figure 6 shows the model-P $S_{Ni-Ni}(Q)$ and $S_{Ni-K}(Q)$ partials and there is a less prominent FSDP in the former and a correspondingly less pronounced trough in the latter, compared to the model-F partials†. To find out what this corresponds to in a 3-D model, the real-space Ni–Ni and Ni–K functions are compared in figure 7. This comparison suggests that modelling the prominent FSDP in the unique $S_{Ni-Ni}(Q)$ partial gives rise to an increase in the number of K^+ ions, and conversely a reduction in the number of metal cations, as next-nearest neighbours to Ni^{2+} ions. This observation is confirmed by comparison of the mean coordination numbers, each averaged over five successive equilibrium configurations, as shown in table 3. Furthermore, as illustrated in figure 7, crudely removing the large FSDP in $S_{Ni-Ni}(Q)$ has the effect in real space of substantially increasing the size of the first (next-nearest-neighbour) peak.

† This is to be expected since a unique Ni–Ni partial can in principle only be obtained if all the isotopic data are used; otherwise RMC modelling will generate a less structured solution.

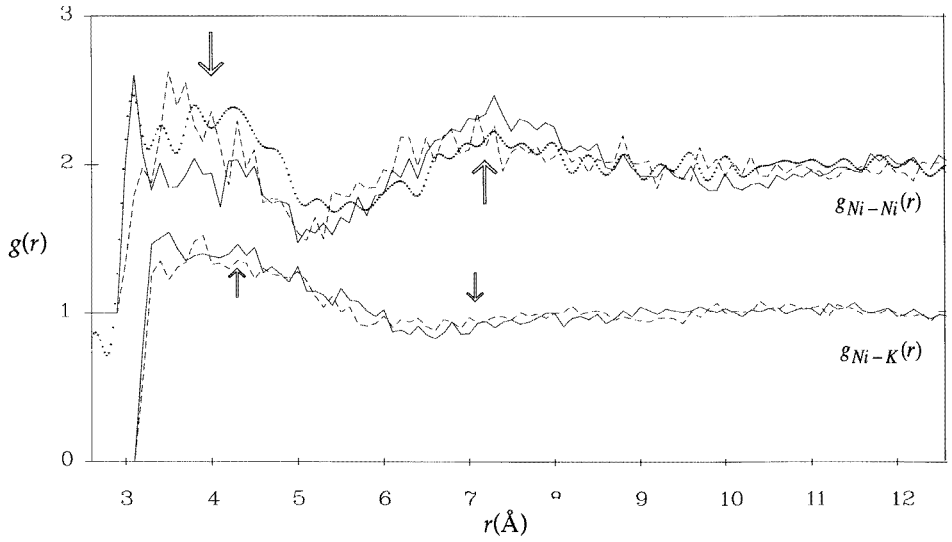

Figure 7. Comparison of Ni–Ni and Ni–K pair distribution functions for RMC models F (solid curves) and P (dashed curves). It is apparent from the changes highlighted by the arrows that modelling the FSDP in the Ni–Ni PSF gives rise to a reduction in the number of Ni^{2+} ions, and conversely an increase in the number of K^+ ions, as next-nearest neighbours to the metal cation. The dotted curve shows the effect in real space of crudely removing the large FSDP in the Ni–Ni PSF prior to Fourier transformation.

Clearly, RMC modelling suggests there is chemical ordering on the length scale of IRO, involving Ni^{2+} and K^+ ions, which is manifest as an anti-phase relationship between the peaks in $S_{Ni-Ni}(Q)$ and $S_{Ni-K}(Q)$ at low Q. This behaviour would seem to mirror the more familiar anti-phase relationship between peaks at $Q \sim 2$ Å^{-1} in the cation–anion and anion–anion PSFs of pure molten salts, which is widely regarded as a signature of the Coulombic nature of interionic forces.

Further insight into the possible origins of the enhanced IRO can be gained from comparison of the bond-angle distributions (again, averaged over several statistically independent RMC configurations) for the two models as shown in figure 8. Modelling the prominent FSDP in $S_{Ni-Ni}(Q)$ leads to pronounced peaks at approximately 90° and 180° in the model-F Ni–Cl–Ni function. That this is consistent with an increase in the proportion of K^+ next-nearest neighbours to Ni^{2+} cations can be visualized from figure 9 which illustrates the likely effect on the conformation of corner-linked and edge-sharing nickel-centred units. There is also some indication from the general depression of the Ni–Ni–Ni function at low angles of a 'straightening out' of linked units. Furthermore, because the main effect in real space of crudely removing the enhanced FSDP in $S_{Ni-Cl}(Q)$ (see figure 10) appears to be to shift the second peak to lower r, a large FSDP in this partial seems to be associated with relatively isolated nickel-centred units and is thus consistent with the concept of more rectilinear, linked chains of such units. Bond network analysis (table 4) also appears to be consistent with this simple picture, with the RMC structures shown to be dominated by branched chains and complex units (containing loops and rings) rather than entities corresponding to discrete $NiCl_4^{2-}$ tetrahedra. Visual inspection of a typical 'slice' through a model-F RMC configuration, as shown in figure 11, confirms this

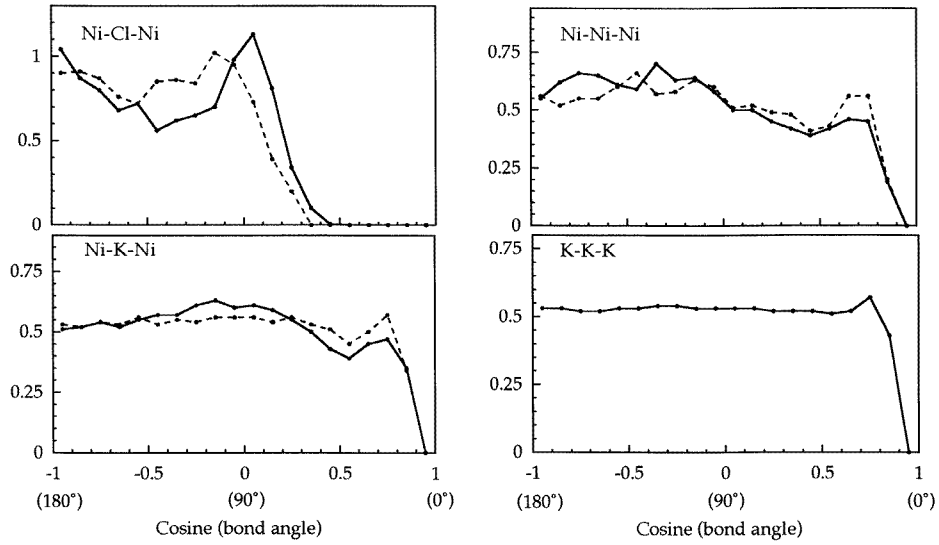

Figure 8. Comparison of RMC bond-angle distributions pertaining to IRO for models F (solid curves) and P (dashed curves).

general impression.

Evidently, RMC modelling suggests that the prominent FSDP in the model-F $S_{Ni-Ni}(Q)$ partial arises (indirectly) from the increased numbers of K^+ ions as next-nearest neighbours to Ni^{2+} ions. This is broadly consistent with, and lends support to, the model suggested in our earlier composition study [1]. However, charge ordering of discrete $NiCl_4^{2-}$ tetrahedral units by the alkali counter-ions is not a significant feature of the RMC model because of the small numbers of such discrete units and the absence of a clear peak at approximately 180° in

Table 4. The results of bond network analysis (averaged over several equilibrium configurations) for the RMC models. The total numbers of branched chains and complex units (containing loops and rings) formed by neighbouring metal cations and anions, separated by no more than 2.8 Å, are shown. The branched chains of five-atom size correspond to discrete tetrahedra. The much greater numbers of such discrete units, in addition to branched chains and complex units, in the mixtures compared to the corresponding pure molten salts is consistent with the 'network-breaker' role of the alkali halide as supported by previous composition studies. Any quantitative differences between the mixtures in the degree of network breakdown, e.g. the smaller number of branched chains in molten $ZnCl_2$–KCl, appear largely to be vestiges of the structural differences between the pure molten salts.

	Branched chains		Complex units
RMC model	All $\geqslant$ three-atom size	Five-atom size	All sizes
$NiCl_2$–KCl P	95	27	15
$NiCl_2$–KCl F	104	35	31
$ZnCl_2$–KCl	68	28	16
Pure $NiCl_2$	25	3	15
Pure $ZnCl_2$	4	0	1

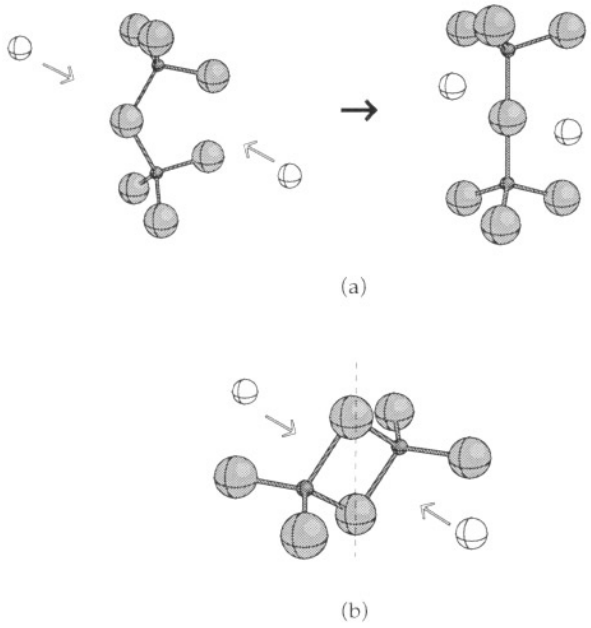

Figure 9. An illustration (exaggerated) of the apparent effect of increased numbers of K^+ ions as next-nearest neighbours to nickel, on the conformation of (a) corner-linked and (b) edge-sharing $NiCl_4^{2-}$ tetrahedral units in molten $NiCl_2$–KCl. The atoms are shown to reduced scale (for clarity) with the large grey spheres representing chlorine, the small grey spheres the nickel and the uncoloured spheres the potassium atoms. The 'bonds' do not imply the existence of actual bonds but simply serve to highlight the geometry of (mainly) ionic complexes. In (a) it can be seen how the large K^+ ions promote a more rectilinear conformation of corner-linked tetrahedral units (although only two linked units are shown, the same will be true of larger linked chains). In (b) a similar process can be seen at work in the case of edge-sharing tetrahedra, where the large K^+ ions limit the movement of the two 'wings' around the axis joining the bridging chlorine atoms (dotted line), thus giving rise to a more symmetrical structure.

the Ni–K–Ni bond-angle distribution (figure 8). The almost featureless K–K–K distribution would seem to imply that the K^+ ions occupy quite disordered sites in the structure. However, the increased order in the model-F Ni–K–Ni bond-angle distribution, compared to that for model P, suggests that the alkali cations do begin to take up ordered positions relative to the Ni^{2+} ions. Thus the featureless K–K–K distribution would actually seem to reflect the random orientation of linked nickel-centred units and the random distribution of such chains with respect to each other. At this stage, it is worth pausing to note two points. Firstly, there is no direct information available from the isotopic data concerning the partials involving potassium, so RMC modelling may simply be underestimating the order in the Ni–K, Cl–K and K–K correlations. Indeed, it should always be borne in mind that the discussion only ever refers to a particular model and that other, perhaps more obviously 'lattice-like' and charge-ordered, structures have not been ruled out. Secondly, the composition is known to fall short of the critical 2/3 alkali halide concentration, which could explain the smaller than expected number of discrete tetrahedral units and hence also why a more strongly charge-ordered RMC structure is not apparent.

The findings from RMC modelling of molten $NiCl_2$–KCl do share some similarities

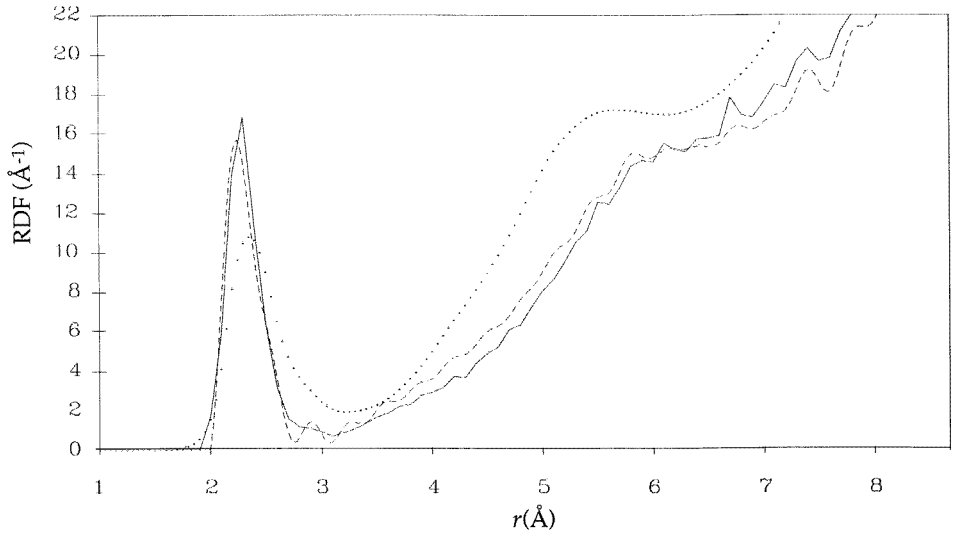

Figure 10. Comparison of the RDFs (defined as $4\pi\rho_0 r^2 g(r)$) for the Ni–Cl correlation. The solid curve is the RDF obtained using the model-F $g_{Ni-Cl}(r)$ function and the dotted curve is the corresponding RDF for pure molten $NiCl_2$ obtained from the data of Newport *et al* [12]. The dashed curve shows the effects in real space of crudely removing the FSDP in the corresponding model-F PSF prior to Fourier transformation.

to those of Börjesson *et al* [13] for fast-ion-conducting glasses. The addition of AgI to a phosphate or borate glass host material gives rise to a proportionate increase in the size of the FSDP at $Q \sim 0.7$ Å^{-1} [14]. RMC modelling by Börjesson and co-workers suggests that the enhanced FSDP arises not from correlations involving the additive, AgI, but from local density fluctuations in the phosphate network stemming from the requirement to maintain the connectivity of oxygen-sharing PO_4 tetrahedral units while the network is being diluted by the increasing salt content.

As regards the local structure of the Ni^{2+} ion, the results indicate that the local coordination is mostly fourfold and almost regularly tetrahedral, in addition to being much better ordered than in pure $NiCl_2$. The average anion coordination, estimated directly from the second-order difference G_7 (figure 5), is approximately 3.6 ± 0.2. A similar mean value of 3.7 ± 0.2 is obtained from RMC modelling, and the distribution (figure 12) suggests that most units are fourfold coordinated (although a sizeable proportion are threefold coordinated). From the position of the first, mainly Ni–Cl, peak at $r \sim 2.28$ Å and the second, mainly Cl–Cl, peak at $r \sim 3.6$ Å in the $G(r)$ data, a r_{--}/r_{+-} ratio of approximately 1.58 is obtained, which is close to the value of $\sqrt{8}/3$ ($\approx$1.63) expected for a regular close-packed tetrahedron. RMC bond-angle distributions (see figures 12 and 13) confirm an almost regularly tetrahedral local geometry for the Ni^{2+} ion. The Cl–Ni–Cl function exhibits a single prominent peak at $\sim$98°. Although this is not very close to the 109.5° expected for a regular tetrahedron, a predominantly octahedral geometry can be ruled out because there is no substantial peak at 180°. The Cl–Cl–Cl function also exhibits a single peak at $\sim$53° which, again, is not far off the expected value of 60° for a regular tetrahedron. The better-ordered local structure is apparent from the comparison of radial distribution functions (RDFs) in figure 10. The Ni–Cl principal peak for molten $NiCl_2$–KCl is clearly much taller, with a reduced FWHM and a deeper first minimum, at lower r,

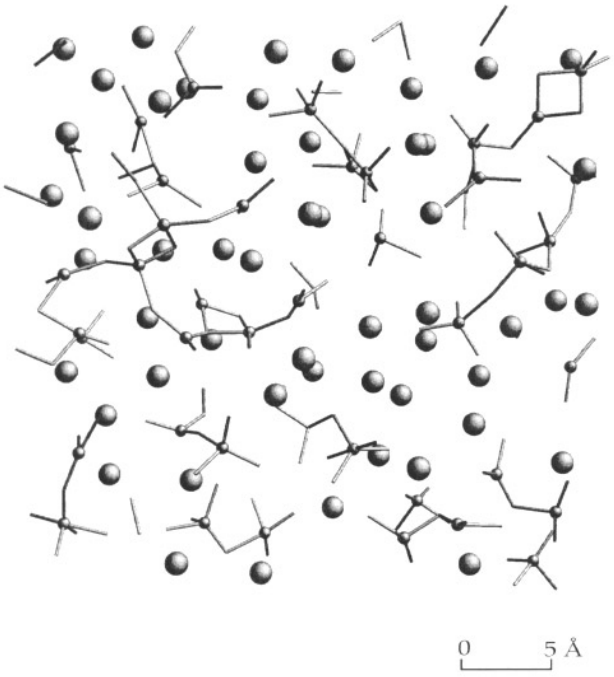

Figure 11. A section (8 Å thick) containing approximately 450 atoms from the middle of a typical RMC model-F equilibrium configuration The small nickel atoms can be readily distinguished from the larger potassium atoms. For clarity, the chlorine atoms are not shown, but their presence can be deduced from the 'bonds' (a purely geometric definition) drawn between all Ni and Cl atoms with separations of less than 3 Å. Note the relatively short chains of nickel-centred units and the disordered distribution of potassium ions.

compared to the case for molten $NiCl_2$. These findings are wholly in accord with those of our earlier composition study [1].

4.2. The structure of molten $ZnCl_2$–KCl

The total structure factors and corresponding total pair distribution functions for the three $ZnCl_2$–KCl molten salt samples are shown in figures 14 and 15, respectively. Attempts were made to model all three data-sets simultaneously using RMC modelling in much the same manner as already described above for the nickel isotopes experiment. Unfortunately, the results (not shown) clearly indicated that the three structure factors were inconsistent with the same RMC structural model and hence with each other. This is borne out from modelling the data using the model-F RMC partials, obtained from fitting the nickel isotopes data, with the appropriate Faber–Ziman coefficients. It can be seen from figure 15 that while a good fit is obtained in real space to the Zn–Cl principal peak at $r \sim 2.3$ Å for the ^{35}Cl-enriched sample, there is an increasingly poor match with the data for the other two samples as the total coherent scattering diminishes. The mismatch, particularly in the case of the weakly scattering ^{37}Cl-enriched sample, is thought to be due to errors in the container correction and associated errors in the normalization of the data. Such errors provide an explanation for there being a good match between model and data in the shape and size of the FSDP

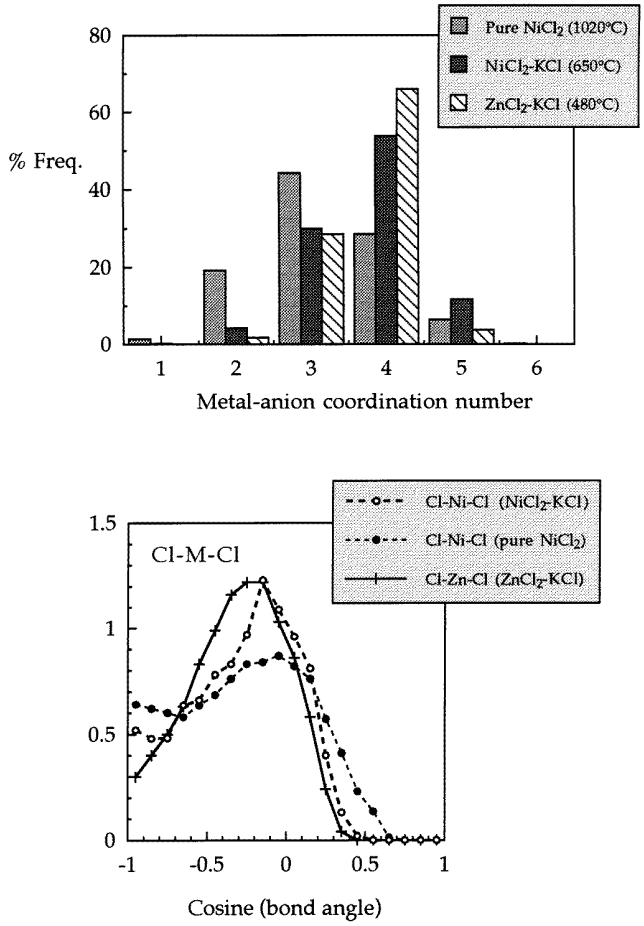

Figure 12. The RMC coordination number and bond-angle distributions relevant to the local structure of the metal (M) cation in $NiCl_2$–KCl and $ZnCl_2$–KCl molten salt mixtures. Comparison is made with the corresponding functions from a RMC configuration (courtesy of R L McGreevy [15]) obtained by modelling isotopic data for pure molten $NiCl_2$ [12].

for the ^{35}Cl-enriched sample but not for the other two samples. The problem arises from using fused quartz, which is not a featureless scatterer, as the sample container material. In Q-space, there is a quartz peak at approximately 1.5 Å^{-1}, so even a small error in the container correction will lead to either a deeper, or shallower, trough on the high-Q side of the FSDP, and this will affect the apparent height and position of that feature—particularly if it is small. Unfortunately, TOF data invariably seem to contain spurious slopes in Q-space, which, combined with the finite statistics at high Q, are manifest as unphysical features at low r in the Fourier transform, and this makes it difficult to use the Si–O principal peak position in quartz of $r \sim 1.6$ Å as a guide to the accuracy of container correction. Given the inconsistencies† between the isotopic data-sets, the rest of this discussion will focus on

† The inconsistencies are confirmed by direct isotopic differencing, which reveals a large peak and a trough, respectively, at $r \sim 2.6$ Å (corresponding to the O–O principal peak position in quartz) in the two second-order differences.

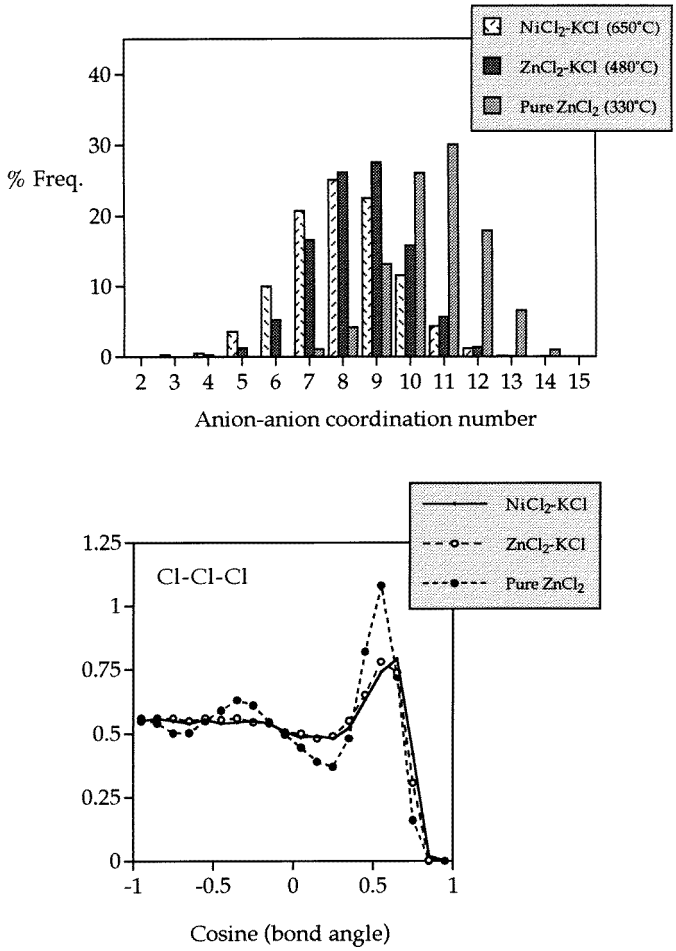

Figure 13. The RMC coordination number and bond-angle distributions pertaining to the anion structure in $NiCl_2$–KCl and $ZnCl_2$–KCl molten salt mixtures. Comparison is made with the corresponding functions from a RMC configuration (courtesy of R L McGreevy [15]) obtained by modelling isotopic data for pure molten $ZnCl_2$ [3].

the data for the ^{35}Cl-enriched sample, which will be least affected by errors in the container correction and for which a RMC structural solution providing an excellent fit in Q-space was also obtained (figure 14).

Again, a random RMC configuration containing $N = 2400$ atoms satisfying the appropriate geometrical constraints was the starting point for modelling the structure factor data (the effective simulation size was approximately 21.6 Å). Initial attempts at modelling indicated an error in composition similar to that encountered with the $NiCl_2$–KCl data. Again, tests suggested that the true composition was closer to 60% KCl—which was adopted in the final RMC model and for modelling using the model-F RMC partials—rather than the nominal 67% KCl. This is not surprising, since the same systematic error leading to KCl-deficient $NiCl_2$–KCl samples is equally likely to affect the $ZnCl_2$–KCl samples. The final RMC solution achieved a best-fit χ^2 of approximately 1.1. The fit in real space can

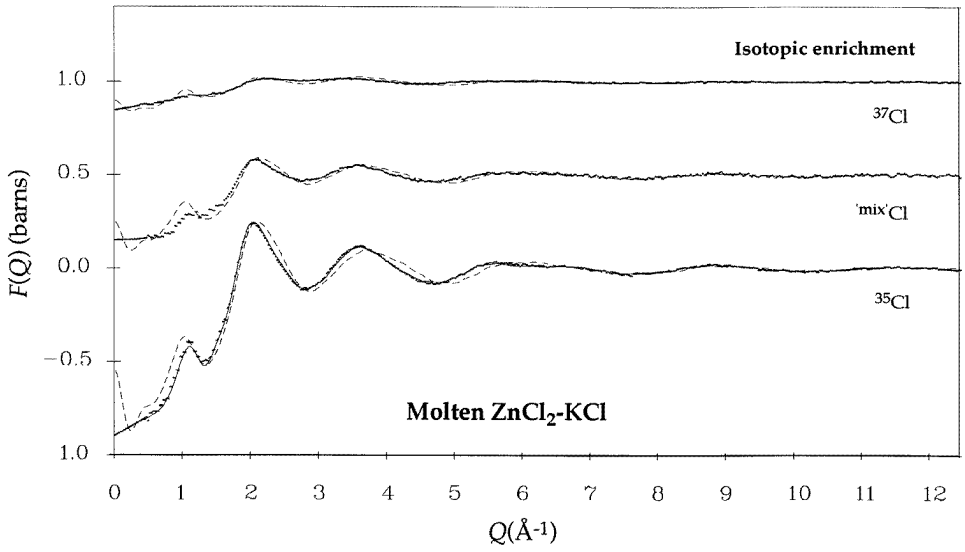

Figure 14. Total structure factors for the three isotopic enrichments of molten $ZnCl_2$–KCl (dotted curves) compared with model $F(Q)$ functions assembled using the RMC partials found from modelling the nickel isotopes data (dashed curves). The model partials were of course weighted with the appropriate Faber–Ziman coefficients (the composition was taken to be 60% KCl in all cases). The RMC fit directly to the ^{35}Cl data is also shown (solid curve).

be seen in figure 15 and although there is some problem in resolving the K–Cl and Cl–Cl partial structures where they overlap at approximately 2.9 Å, the RMC solution generally provides a good match to the data. As usual, several statistically independent equilibrium configurations were collected for averaging of their structural properties.

At this point, the alert reader may question whether anything of significance could be learned from an RMC model obtained by fitting to a single structure factor for a system which has six partial structures. However, as we shall see, particularly from the comparison of RMC results for the local structure with those of pure $ZnCl_2$, RMC modelling does seem able to extract significant amounts of information from the ^{35}Cl data. Furthermore, the interesting results realized and the good agreement achieved with the results of earlier composition studies amply justify, in our opinion, the detailed discussion which follows.

RMC coordination number and bond-angle distributions relevant to the local structure of the metal cation are shown in figure 12, and these indicate a regular tetrahedral geometry just as in pure molten $ZnCl_2$. The mean anion coordination of Zn^{2+} ions is approximately 3.7 ± 0.1, with the fourfold coordination being most likely. The Cl–Zn–Cl bond-angle distribution peaks (almost symmetrically) around 104° and is little different to that obtained by RMC modelling for pure $ZnCl_2$†. The principal Zn–Cl and Cl–Cl peak positions in $G(r)$ of ∼2.3 and 3.7 Å, respectively, are also little different, and confirm a similar r_{--}/r_{+-} ratio of ∼1.61. In addition, the height of the Zn–Cl principal peak in the RDF of approximately 18 ± 1 does not differ markedly from that for pure $ZnCl_2$. Clearly, the results seem to confirm the persistence of the $ZnCl_2$ local structure in the mixtures as suggested by Allen

† Note that because a complete set of isotopic data were used to produce the RMC model for pure $ZnCl_2$, the close similarities with the current RMC results for local structure, in particular the highly ordered Cl–Zn–Cl bond-angle distribution, imply that RMC modelling is extracting some significant information from the ^{35}Cl data.

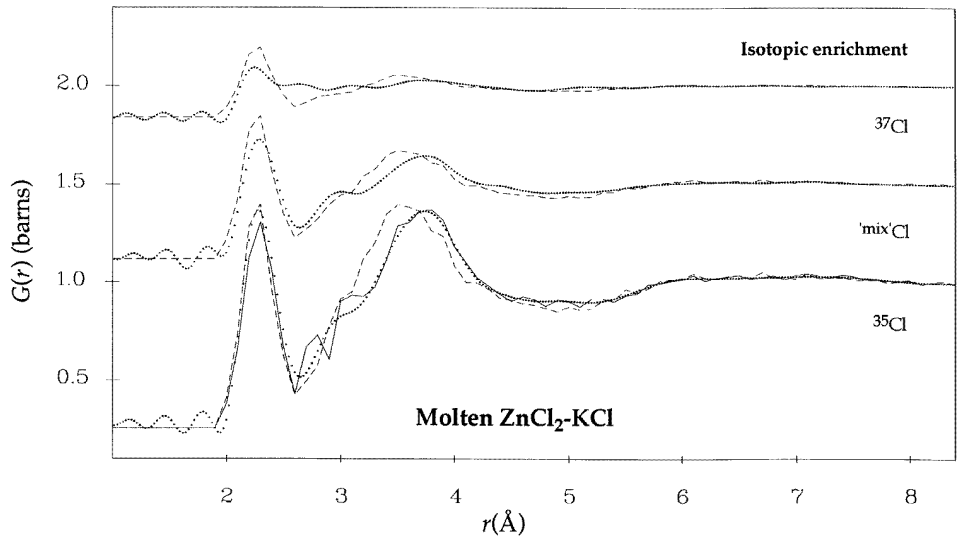

Figure 15. Total pair distribution functions for the three isotopic enrichments of molten $ZnCl_2$–KCl (dotted curves) compared against the model functions (dashed curves) assembled from the RMC partials obtained for the nickel isotopes data. The mismatch between the model and the data for the ^{37}Cl-enriched sample, especially in the region of the first minimum at approximately 2.7 Å, clearly suggests a problem with the correction for container scattering. The real-space RMC fit to the data for the ^{35}Cl-enriched sample is also shown (solid curve).

et al [2]. Furthermore, the lack of change in the position of the Cl–Cl principal peak in the $ZnCl_2$–KCl mixtures, in contrast to the shift to high r observed in the case of molten $NiCl_2$–KCl, is consistent with the suggestion made in our earlier composition study [1] that the local geometry of the metal cation in pure molten $NiCl_2$ is dissimilar to that in pure $ZnCl_2$. As regards the anion structure, our findings must be more tentative in view of the restricted information available to RMC modelling (indeed, the very purpose of the isotopic substitution had been to obtain detailed information about the anion structure). The coordination number distribution in figure 13 shows a dramatic reduction in density compared to the case of molten $ZnCl_2$, with the mean coordination number falling from ∼10.6 down to ∼8.5. Molten $ZnCl_2$–KCl does not appear to retain the dense, close-packed anion structure of the pure salt (a similar change does not occur in the case of the $NiCl_2$–KCl melts, probably because the anion structure in pure molten $NiCl_2$ is much less dense to begin with). This is not surprising given the evidence for the breakdown of the 'network liquid' structure of pure $ZnCl_2$ upon the addition of alkali halide (see [2] and references therein). The loss of connectivity appears to be confirmed by the disappearance of the peak present at ∼107, and the diminution of the peak at ∼57, in the Cl–Cl–Cl bond-angle distribution for pure $ZnCl_2$. Note that the apparent reduction in external constraints on the linkage of tetrahedral $ZnCl_4^{2-}$ units seems to have little effect on the local structure of the Zn^{2+} cation, which appears remarkably stable and resilient.

In order to discuss intermediate-range order, it is necessary to turn to modelling and make comparisons with the results for molten $NiCl_2$–KCl. From figure 14, it can be seen that the FSDP in the structure factor for the ^{35}Cl-enriched sample is of a similar size and shape to the model FSDP but is positioned at slightly higher Q and appears to be somewhat

narrower. Firstly, this implies a strong similarity between the two systems as regards intermediate-range order. Secondly, the relative sharpness and position of the feature in molten $ZnCl_2$–KCl may possibly reflect the more efficient packing possible in this case due to the better-ordered, more regularly tetrahedral local structure of the Zn^{2+} cation.

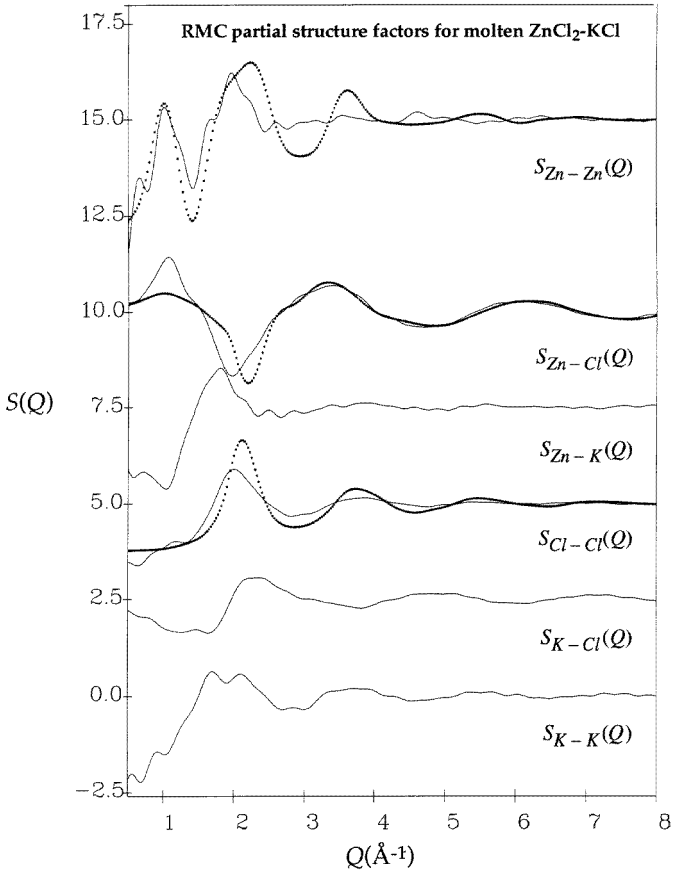

Figure 16. RMC partial structure factors for molten $ZnCl_2$–KCl obtained from fitting the $F(Q)$ data for the ^{35}Cl-enriched sample (solid curves). Partial structure factors for pure molten $ZnCl_2$, from the isotopic study by Biggin and Enderby [3], are also shown (dotted curves).

In general, a strong similarity between the structures of the two molten salt systems is suggested by the excellent match between the amplitudes of all the main peaks in the total structure factors for model and data. The RMC partial structures for molten $ZnCl_2$–KCl (figure 16) are also very similar to those for model F (figure 6) especially in the case of those PSFs which contribute most to the total scattering†. In addition, the bond-angle and coordination number distributions (figures 12 and 13) suggest nearly similar local and anion structures. Any remaining differences between the mixtures appear largely to be vestiges of the dissimilar pure salt structures. For example, the Cl–Ni–Cl bond-angle distribution in figure 12, when compared to the Cl–Zn–Cl distribution, appears to be slightly skewed

† Again, note that this also implies that RMC modelling is managing to extract a significant amount of information from, in this case, just a single structure factor.

towards that expected of an octahedral geometry. Differences in the results of bond network analysis (see table 4) can also be interpreted as arising from the dissimilar pure salt structures. The general similarity between the two molten salt systems is perhaps not surprising given the almost identical ion sizes of the two metal species. However, this naturally begs some questions as to the reasons for the clearly different structures of the pure salts, which are considered (briefly) next.

4.3. The structures of the pure $ZnCl_2$ and $NiCl_2$ melts

The Zn^{2+} cation has been found to have a tetrahedral coordination in crystalline polymorphs of pure $ZnCl_2$ and in the glass phase [16]. In contrast, the Ni^{2+} cation has an octahedral coordination within a layered $CdCl_2$-type structure, in the crystalline phase of pure $NiCl_2$ [17]. RMC modelling by McGreevy and Pusztai [15] suggests that, in common with a range of other monovalent and divalent metal halide salts studied, the $ZnCl_2$ and $NiCl_2$ melts retained the basic local symmetries of the corresponding crystals from which they fused. This conclusion is, of course, wholly consistent with the current findings and our earlier composition study [1]. Obviously, to explain the differing structures, effects other than simple ion size must be invoked. From a neutron diffraction study of the nickel halides, Wood and Howe [4] suggested a model involving reduced charge transfer arising from hybridization of the metal d band and anion p band. The electronic structure of Ni^{2+} is d^8, and is therefore quite different to that of Zn^{2+} which has a completely filled d shell. It appears very likely that such differences play a part in determining structure. Indeed, it has been suggested [18] that the large deficit in the entropy of melting of pure $ZnCl_2$ is associated with the persistence of a strong network of partially covalent bonds arising from hybridization of d states on Zn^{2+} with p states on Cl^-. More recently, Wilson and Madden [19] have put forward a simple ionic model which includes the effect of induced dipoles on the structure of divalent metal halide melts consisting of a small, highly polarizing cation and a large, highly polarizable anion, such as $ZnCl_2$. Computer simulation [20] shows that this polarizable anion model, unlike those based upon a rigid-ion assumption, can reproduce observed experimental features such as the overlap of principal peaks in $g_{++}(r)$ and $g_{--}(r)$ as well as the FSDP in $S_{++}(Q)$. However, given the almost identical metal-ion sizes, it seems unlikely that the differences in structure of $ZnCl_2$ and $NiCl_2$ can be explained simply by including polarization effects in a simple ionic model. It still seems necessary to invoke 'covalency' effects arising from the detailed electronic configuration as an explanation for the different melt structures and for such non-Coulombic features as adjacent layers of anions in the $CdCl_2$ structure of crystalline $NiCl_2$.

5. Summary

The general trends in structural modification for $NiCl_2$–KCl molten salt mixtures, first identified in the earlier composition study, have been confirmed by isotopic substitution of the nickel species at a specific composition. RMC modelling of the isotopic data-sets has made it possible to ensure a physically consistent set of PSFs. The unique $S_{Ni-Ni}(Q)$ partial obtained in this manner exhibits, unlike the corresponding PSF for molten $NiCl_2$, a prominent FSDP, thus confirming the existence of enhanced IRO in the mixtures. The RMC findings also confirm a better-ordered, more regularly tetrahedral local structure around the Ni^{2+} ion and the dominance of the anion structure by the metal cation. Comparison of RMC models obtained by fitting to all or part of the isotopic data has made it possible to identify the structural features arising from modelling the prominent FSDP in $S_{Ni-Ni}(Q)$.

The results suggest that the enhanced IRO in the mixtures arises from increased numbers of K^+ ions as next-nearest neighbours to Ni^{2+} ions. This is broadly consistent with, and lends support to, the model suggested in our earlier composition study in which the alkali cation plays a central role in promoting IRO. Although it was not possible to obtain detailed information about the anion structure in molten $ZnCl_2$–KCl, RMC modelling of the structure factor for the most strongly scattering ^{35}Cl enrichment did confirm the persistence of the tetrahedral $ZnCl_2$ local structure. Modelling also confirmed the general similarity to molten $NiCl_2$–KCl, with any residual differences between the two molten salt systems appearing largely to be vestiges of the dissimilar structures of the pure $NiCl_2$ and $ZnCl_2$ melts.

The somewhat narrower FSDP at slightly higher Q in molten $ZnCl_2$–KCl, compared to that in molten $NiCl_2$–KCl, hints at the importance of well-ordered local units as regards IRO in the mixtures. In this context, a recently published study of structural modification in alkali chloro-aluminate melts [21] is of particular interest.

Acknowledgments

We would like to thank the staff at the Rutherford ISIS facility, particularly W S Howells, for their assistance in data collection and analysis. We are grateful to R L McGreevy and J D Wicks for supplying the RMC software and providing much advice about its use. Thanks also to the Bristol isotope preparation unit, and to Phil Mitchell and Sherilyn Wass of Reading University, for assistance with sample preparation. As always, we gratefully acknowledge the continued support given to this work by the Science and Engineering Research Council, and in particular Y S Badyal would like to thank the SERC for awarding him a studentship.

References

[1] Badyal Y S and Howe R A 1993 *J. Phys.: Condens. Matter* **5** 7189
[2] Allen D A, Howe R A, Wood N D and Howells W S 1992 *J. Phys.: Condens. Matter* **4** 1407
[3] Biggin S and Enderby J E 1981 *J. Phys. C: Solid State Phys.* **14** 3129
[4] Wood N D and Howe R A 1988 *J. Phys. C: Solid State Phys.* **21** 3177
[5] Faber T E and Ziman J M 1965 *Phil. Mag.* **11** 153
[6] Bazhenov V M, Raspopin S P and Chervinskii Y F 1984 *Russ. J. Inorg. Chem.* **29** 1814
[7] Perry G S, Macdonald L G and Newstead S 1983 *Thermochim. Acta* **68** 341
[8] Soper A K, Howells W S and Hannon A C 1989 ATLAS—analysis of time-of-flight diffraction data from liquid and amorphous samples *RAL Report* RAL-89-046
[9] Soper A K 1992 private communication
[10] Sears V F 1992 *Neutron News* **3** 26
[11] McGreevy R L and Howe M A 1991 *Phys. Chem. Liq.* **24** 1
[12] Newport R J, Howe R A and Wood N D 1985 *J. Phys. C: Solid State Phys.* **18** 5249
[13] Börjesson L, McGreevy R L and Howells W S 1992 *Phil. Mag.* B **65** 261
[14] Börjesson L, Torrel L M, Dahlborg U and Howells W S 1989 *Phys. Rev.* B **39** 3404
[15] McGreevy R L and Pusztai L 1990 *Proc. R. Soc.* **430** 241
[16] Desa J A E, Wright A C, Wong J and Sinclair R N 1982 *J. Non. Cryst. Solids* **51** 57
[17] Wyckoff R W G 1963 *Crystal Structures* 2nd edn, vol 1 (New York: Interscience)
[18] Akdeniz Z and Tosi M P 1992 *Proc. R. Soc.* A **437** 85
[19] Wilson M and Madden P A 1994 *J. Phys.: Condens. Matter* **6** A151
[20] Wilson M and Madden P A 1993 *J. Phys.: Condens. Matter* **5** 6833
[21] Badyal Y S, Allen D A and Howe R A 1994 *J. Phys.: Condens. Matter* **6** 10 193